Preprint typeset in JHEP style

Non-metricity signatures on the Higgs boson signal strengths at the LHC

Victor Ilisie[a]

[a] *Escuela de Ciencias, Ingeniería y Diseño, Universidad Europea de Valencia, Paseo de la Alameda 7, 46010, València, Spain*

E-mail: victor.ilisie@universidadeuropea.es

Abstract: In this work we study the high-energy Higgs boson phenomenology associated to the non-metricity scale Λ_Q at the LHC. Non-metricity is present in more generic non-Riemannian geometries describing gravity beyond General Relativity and exhibits nice features in astronomy and cosmology, and it can be analysed perturbatively. Using effective field theory tools, we calculate the *new physics* contributions to the one-loop $H \to \gamma\gamma$ and $gg \to H$ processes and, together with previous bounds from Compton scattering, we obtain relevant constraints and correlations in the model's parameter space. This can help us take a step further, and no longer associate gravitational effects uniquely to astronomical phenomena, and to start analysing these effects by means of high energy experiments. In turn, this could also help us get a better grasp at quantum phenomena associated to gravity.

Contents

1 Introduction

With the discovery of the Higgs boson [1, 2] the Standard Model (SM) has proven once more its success. Even though the latest provided data seem to be extraordinarily consistent with its predictions [3–29] its discovery has left many open questions, such as, the need for additional CP violation in order to explain the matter-antimatter asymmetry in the Universe, the lack of candidates for dark matter and dark energy, the Higgs and quark hierarchy problem, just to name a few. As there is no fundamental principle that forbids us from extending this model, in the last few decades a large number of SM extensions have been proposed and analysed and, using the available experimental data, important bounds have been set on their parameter space. Nonetheless, if one does not wish to compromise with a specific extension, one can embed the SM Lagrangian into a generic effective field theory (EFT) Lagrangian as it has been extensively analysed in the literature [30–45] i.e.,

$$\mathcal{L}_{\rm EFT} = \mathcal{L}_{\rm SM} + \sum_{k,j} \frac{c_j^{(k)}}{\Lambda^k} \mathcal{O}_j^{(k)} \,, \tag{1.1}$$

where $k \geqslant 1$ is the power corresponding to some new physics scale Λ (given in mass units). The $c_j^{(k)}$ terms are the so-called Wilson coefficients and, $\mathcal{O}_j^{(k)}$ the operators built in terms

of the SM fields, both corresponding to the $1/\Lambda^k$ term of the expansion. As it is already well known, the only drawback is that the previous expansion is infinite and therefore non-renormalizable. However, once the power series is *cut* at some power k', the corresponding $\mathcal{L}_{\text{EFT}}$ Lagrangian is renormalizable in the usual sense [45].

On the other hand, in a very similar situation we find General Relativity (GR). It has repeatedly proven its success over the past decades, and perhaps one of the most outstanding predictions, verified experimentally in the last years, is the existence of gravitational waves [46–54]. Let us, however, comment on its theoretical structure and explain how, just as in the SM model case, it can be embedded in a larger and more generic framework. First of all, at the time GR was born, only Riemannian geometry was known, and so the model was built upon the metricity assumption i.e.,

$$\nabla_\mu \, g_{\alpha\beta} = 0 \,, \tag{1.2}$$

where ∇_μ is the covariant derivative and $g_{\alpha\beta}$ the metric components. However, nowadays we know that, for a generic manifold, given a metric g and a connection Γ, we can define the non-metricity (Q), curvature (R) and torsion (S) tensors as three independent quantities, as it is nicely described in [55]

$$\begin{aligned} Q_{\mu\nu\rho} &= \nabla_\nu \, g_{\nu\rho} \,, \\ R^\rho{}_{\lambda\nu\mu} &= \Gamma^\rho{}_{\mu\lambda,\nu} - \Gamma^\rho{}_{\nu\lambda,\mu} + \Gamma^\rho{}_{\nu\alpha}\Gamma^\alpha{}_{\mu\lambda} - \Gamma^\rho{}_{\mu\alpha}\Gamma^\alpha{}_{\nu\lambda} \,, \qquad (1.3) \\ S_{\mu\nu}{}^\rho &= \frac{1}{2}\left(\Gamma^\rho{}_{\mu\nu} - \Gamma^\rho{}_{\nu\mu}\right) \,, \qquad (1.4) \end{aligned}$$

where $\Gamma^\rho{}_{\mu\lambda,\nu} \equiv \partial_\nu \, \Gamma^\rho{}_{\mu\lambda}$, with ∂_ν the ordinary partial derivative and $\Gamma^\mu{}_{\nu\alpha}$ the components of the connection Γ in a given basis. Note therefore, that GR in its original form is just a particular case for which $Q = S = 0$ and, as a consequence, the connection Γ can be written in terms of the metric tensor and its first (ordinary) derivatives.

Thus, again, just as in the case of the SM, as there is no fundamental principle that forbids us to extend GR, we can embed it into more generic geometrical theories that allow for non-vanishing torsion and non-metricity, and constrain these terms experimentally, as it is currently done in high energy particle physics. Depending on the specific characteristics of S and Q, many models have been discussed and analyzed in the literature, such as [56–71], just to mention a few.

Here, we are going to focus on Ricci-based gravity (RBG) models [72] and their high energy phenomenology at the LHC. These models are strongly motivated from a physical point of view [72–79] and also, they result appealing as they can be treated perturbatively within an effective field theory framework [79].

In this paper, we are going to briefly introduce the RBG action and its expansion in powers of the non-metricity scale, and use it to calculate the effective Lagrangian corresponding to the $H\bar{f}f\gamma\gamma$ and $\bar{f}f\gamma\gamma$ vertices, where f is an arbitrary fermion (with or without electric charge), H the Higgs boson and γ, a photon. Afterwards we will use this Lagrangian to recalculate the modified Compton cross section $\sigma_{\gamma e\to\gamma e}$ including non-

metricity effects.[1] The same Lagrangian will also be used for calculating the relevant Higgs decay and productions channels and the corresponding LHC signal strengths, again including modifications induced by the non-metricity scale. Finally, we will perform a phenomenological analysis comparing the model predictions with the currently available experimental data and extract bounds on the parameters of the model.

2 Ricci-based Gravity Theories and EFTs

As it was recently pointed out [72, 75–77], there is a broad class of higher-order curvature theories that are characterized by non-trivial non-metricity tensors. In these studies, for a broad subset of the previously mentioned theories i.e., Ricci-based gravity theories, it was found that the presence of non-metricity can induce perturbative effective interactions for fields with spin 0, 1/2 and 1. Within this class, there is a sub-class formed by projective-invariant RBG theories, that only include the symmetric part of the Ricci tensor.[2] The action, for this last sub-class of RBG theories, can be generically written as

$$S_{\rm RBG} = \frac{1}{2\kappa}\int d^4x\sqrt{-g}F_{\rm RBG}[g_{\mu\nu}, R_{(\mu\nu)}, \Lambda_{\rm RBG}] + S_{\rm M}[g_{\mu\nu}, \Psi, \Gamma^{\alpha}{}_{\mu\nu}]\,, \tag{2.1}$$

where $F_{\rm RBG}$ is an analytic function of $g_{\mu\nu}$, $R_{(\mu\nu)}$ and $\Lambda_{\rm RBG}$, with $\kappa = M_{\rm Pl}^{-1}$ and with $M_{\rm Pl}$ Plank's mass. The $\Lambda_{\rm RBG}$ factor is the scale at which deviations form GR come into the game, $R_{(\mu\nu)}$ is the symmetric part of the Ricci tensor and $S_{\rm M}$, the action containing the matter fields Ψ (Ψ stands for a generic matter field of arbitrary spin and mass). The non-metricity scale Λ_Q is given by $\Lambda_Q = \sqrt{M_{\rm Pl}\,\Lambda_{\rm RBG}}$, which corresponds to the scale at which the deviations from GR become non-perturbative.

It has been proven[72, 75–77] that the action S admits a representation, the Einstein frame representation, where the gravitational sector is described by standard GR for a metric $q_{\mu\nu}$ and where, the matter sector is minimally coupled to gravity. In general, we can relate the metric tensor $g_{\mu\nu}$ corresponding to an arbitrary frame to the Einstein frame metric tensor, through the so-called deformation matrix Ω given by

$$q_{\mu\alpha}\,(\Omega^{-1})^{\alpha}{}_{\nu} = g_{\mu\nu}. \tag{2.2}$$

The deformation matrix is an on-shell function of the stress-energy tensor and can be expanded in powers of $1/\Lambda_Q^4$ as

$$(\Omega^{-1})^{\alpha}{}_{\nu} = \delta^{\alpha}{}_{\nu} + \frac{1}{\Lambda_Q^4}\left(\alpha\, T\,\delta^{\alpha}{}_{\nu} + \beta\, T^{\alpha}{}_{\nu}\right) + \mathcal{O}(\Lambda_Q^{-8})\,, \tag{2.3}$$

where α and β are arbitrary parameters to be constrained experimentally, as well as Λ_Q. The quantities $T^{\alpha}{}_{\nu}$ and T are the stress-energy tensor and its trace, and the first $\delta^{\alpha}{}_{\nu}$ term

[1] As we shall see in the following, our result does not agree with the one obtained in [76], and we shall re-perform the phenomenological analysis presented therein in terms of the correct expression for the cross section.

[2] It has been shown that, introducing the antisymmetric part of the Ricci tensor, generates ghostly degrees of freedom which present additional physical complications[80–83] and we shall not consider such cases in our analysis.

guarantees that GR is recovered as the low energy limit of the RBG model. We thus obtain, including terms of $\mathcal{O}(\Lambda_Q^{-4})$

$$g_{\mu\nu} = q_{\mu\nu} + \frac{1}{\Lambda_Q^4}\left(\alpha\, T\, \delta^{\alpha}{}_{\nu} + \beta\, T^{\alpha}{}_{\nu}\right) . \tag{2.4}$$

Furthermore, for weak gravitational fields we can expand $q_{\mu\nu}$ about the Minkowskian metric simply as

$$q_{\mu\nu} = \eta_{\mu\nu} + \delta q_{\mu\nu}, \tag{2.5}$$

where $\delta q_{\mu\nu}$ encodes the Newtonian and post-Newtonian corrections to the metric (long range gravitational effects) that can be ignored for high-energy experiments on the Earth's surface.

In the previously introduced generic action (2.1) we have not specified explicitly the functions $\mathrm{F_{RBG}}$ nor the $\mathrm{S_M}$ content. In this sense, particular cases of RBG models, that are worth mentioning, are the Born-Infeld (BI) [72, 73, 78, 84] modification of the QED action

$$S_{\mathrm{BI}} = \beta^2 \int d^4x \left(1 - \sqrt{1 + 2\beta^{-2} F_{\mu\nu}F^{\mu\nu} - 16\beta^{-4}\left(F_{\mu\nu}\tilde{F}^{\mu\nu}\right)^2}\right) , \tag{2.6}$$

that was proposed to avoid the divergent self-energy problem of point charges in classical field theory, and the Eddington-inspired-Born-Infeld (EiBI) model [73]

$$S_{\mathrm{EiBI}} = \pm\Lambda_Q^4 \int d^4x \left(\sqrt{-\left|g_{\mu\nu} \pm \Lambda_{\mathrm{EiBI}}^{-2} R_{(\mu\nu)}(\Gamma)\right|} - \lambda\sqrt{-|g_{\mu\nu}|}\right) , \tag{2.7}$$

which combines Eddington affine gravity with ideas from BI electromagnetism, where $\beta = \pm 1$, the sign in front of Λ_Q. In this last case Λ_Q is related to Λ_{EiBI} by $\Lambda_Q = \sqrt{M_{\mathrm{Pl}}\,\Lambda_{\mathrm{EiBI}}}$. EiBI gravity exhibits nice features as it can yield non-singular solutions for different scenarios in cosmology and astrophysics. Similar to the work presented in [68], we will extract and reinterpret the bounds obtained in our study also in terms of the EiBI model.

3 The effective $(H)\bar{f}f\gamma\gamma$ vertices

Using the previous results, following similar procedures as in [76, 77], we will deduce the effective Lagrangian corresponding to the $H\bar{f}f\gamma\gamma$ and the $\bar{f}f\gamma\gamma$ vertices, that will be used for recalculating the modified Compton Cross section $\sigma_{\gamma e\to\gamma e}$ and for calculating the Higgs signal strengths at the LHC.

Let us start by considering the following Lagrangian that corresponds to a massive Dirac fermion (which can be either charged or neutral), the kinetic term for the photon field, and the Yukawa interaction Lagrangian with all its terms in a curved space-time background i.e., with a generic metric $g^{\mu\nu}$:

$$\begin{aligned}\mathcal{L}_{\mathrm{eff}} = \sqrt{-g}\Bigg[\frac{i}{2}e_a{}^{\mu}\left(\bar{\psi}\gamma^a\nabla_\mu\psi - (\nabla_\mu\bar{\psi})\gamma^a\psi\right) - m\bar{\psi}\psi \\ + \frac{1}{4}g^{\mu\nu}g^{\alpha\beta}F_{\mu\alpha}F_{\nu\beta} - \frac{m}{v}H\bar{\psi}\psi\Bigg] ,\end{aligned} \tag{3.1}$$

where $\nabla_\mu = \partial_\mu - \Gamma_\mu - B_\mu$, with Γ_μ the spinor connection

$$\Gamma_\mu = \frac{i}{2}\omega_\mu{}^{ab}\frac{\sigma_{ab}}{2}\,, \qquad \sigma_{ab} = \frac{i}{2}(\gamma_a\gamma_b - \gamma_b\gamma_a)\,, \tag{3.2}$$

and where B_μ stands for the contributions of arbitrary gauge fields. As usual, the tetrads are given by $g^{\mu\nu} = e_a{}^\mu e_b{}^\nu \eta^{ab}$ with η^{ab} the flat Minkowski metric. Expanding the tetrads $e_a{}^\mu$ up to $\mathcal{O}(\Lambda_Q^{-4})$, neglecting suppressed torsion effects [76, 77] induced by Γ_μ, and also Newtonian and post-Newtonian corrections to the metric, we obtain

$$e_a{}^\mu = \delta_a{}^\mu - \frac{1}{2\Lambda_Q^4}(\alpha\, T^{(J)}\delta_a{}^\mu + \beta\, T_a^{(J)\mu})\,. \tag{3.3}$$

Therefore, the expression for the metric including perturbation terms reads

$$g^{\mu\nu} = \eta^{\mu\nu} - \frac{1}{\Lambda_Q^4}(\alpha\, T^{(J)}\eta^{\mu\nu} + \beta T^{(J)\mu\nu})\,, \tag{3.4}$$

where $T_a^{(J)\mu}$ (or equivalently $T^{(J)\mu\nu}$) and $T^{(J)}$ are the stress-energy tensor and its trace for a spin-J field.

In this analysis, besides tree-level processes we are also interested in calculating loop-induced ones. The results in this last case will be UV-divergent and will, therefore, need renormalization. In order to regularize these divergences we will work in $\mathcal{D} = 4+2\epsilon$ dimensions with $\epsilon < 0$, $|\epsilon| \ll 1$. To insure that we do not miss out possible finite contributions, as the previous terms of the interaction Lagrangian contain metric contractions, we will work in $\mathcal{D}$ dimensions already at the Lagrangian level. Using $\eta_{\mu\nu}\,\eta^{\mu\nu} = \mathcal{D}$ the expansion for $\sqrt{-g}$, up to $\mathcal{O}(\Lambda_Q^{-4})$, reads

$$\sqrt{-g} = \sqrt{-\eta}\left(1 + \frac{1}{2}\,\frac{\alpha\, T^{(J)}\eta^\mu_\mu + \beta\, T^{(J)\mu}_\mu}{\Lambda_Q^4}\right) = 1 + \frac{\mathcal{D}\alpha + \beta}{2\Lambda_Q^4}T^{(J)}\,. \tag{3.5}$$

Inserting the expressions (3.3-3.5) into (3.1) and keeping terms up to $\mathcal{O}(\Lambda_Q^{-4})$ we get

$$\mathcal{L}_{\text{eff}} = \frac{i}{2}\bar\psi \overleftrightarrow{\not D}\psi - m\bar\psi\psi + \frac{1}{4}F^{\mu\nu}F_{\mu\nu} - \frac{m}{v}H\bar\psi\psi + \mathcal{L}^{\text{eff}}_{(1/2)} + \mathcal{L}^{\text{eff}}_{(1)} + \mathcal{L}^{\text{eff}}_{(0)}\,, \tag{3.6}$$

where $D_\mu = \partial_\mu - B_\mu$, $\not D = \gamma^\mu D_\mu$ and $\bar\psi \overleftrightarrow{\not D}\psi = \bar\psi\gamma^\mu D_\mu\psi - (D_\mu\bar\psi)\gamma^\mu\psi$.

Taking $J = 1$ for the expansion of the tetrads and the $\sqrt{-g}$ term for the Dirac Lagrangian, $J = 1/2$ for the expansion of the metric and the $\sqrt{-g}$ term for the photon field Lagrangian, and finally, $J = 1$ for the expansion of $\sqrt{-g}$ for the Yukawa term, we obtain in flat Minkowsky space-time the complete set of interactions corresponding to the $H\bar f f\gamma\gamma$ and $\bar f f\gamma\gamma$ vertices. Their expressions are given by the sum of the three effective interaction

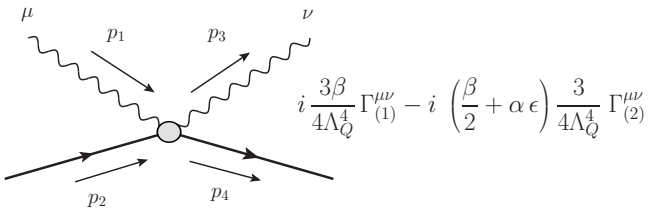

Figure 1. Feynman rule corresponding to the $\bar{f}f\gamma\gamma$ effective interaction vertex and the corresponding four-momentum configuration.

Lagrangians $\mathcal{L}_Q^{\text{eff}} = \mathcal{L}_{(1/2)}^{\text{eff}} + \mathcal{L}_{(1)}^{\text{eff}} + \mathcal{L}_{(0)}^{\text{eff}}$ (see Appendix A)[3] that explicitly reads

$$\begin{aligned}\mathcal{L}_Q^{\text{eff}} = \frac{3\,i\,\beta}{4\Lambda_Q^4}\,F^{\mu\alpha}F^{\nu}{}_{\alpha}\left(\bar{\psi}\gamma_\mu\partial_\nu\psi - (\partial_\nu\bar{\psi})\gamma_\mu\psi\right) - \left(\frac{\beta}{2}+\alpha\,\epsilon\right)\frac{3}{4\Lambda_Q^4}m\bar{\psi}\psi\,F_{\alpha\beta}F^{\alpha\beta} \\ - \epsilon\,(4\alpha+\beta)\,\frac{m}{v}\,\frac{1}{4\Lambda_Q^4}H\bar{\psi}\psi\,F_{\alpha\beta}F^{\alpha\beta}\,.\end{aligned} \tag{3.7}$$

One should note that, having extended the Lagrangian to $\mathcal{D}$ dimensions by using dimensional regularization, we will obtain additional contributions proportional to both α and β in the considered loop diagrams.

The corresponding Feynman rule for the new $\bar{f}f\gamma\gamma$ interaction term is shown in figure 1, where $\Gamma^{\mu\nu}_{(1)}$ and $\Gamma^{\mu\nu}_{(2)}$ explicitly read

$$\begin{aligned}\Gamma^{\mu\nu}_{(1)} &= \eta^{\mu\nu}\,A - \not{p}_1\,p_3^\mu(p_2^\nu+p_4^\nu) - \not{p}_3\,p_1^\nu(p_2^\mu+p_4^\mu) - p_1^\nu\,\gamma^\mu B \\ &\quad - p_3^\mu\,\gamma^\nu C + \gamma^\mu(p_2^\nu+p_4^\nu)(p_1\cdot p_3) + \gamma^\nu(p_2^\mu+p_4^\mu)(p_1\cdot p_3)\,, \\ \Gamma^{\mu\nu}_{(2)} &= 4m\,(\eta^{\mu\nu}\,p_1\cdot p_3 - p_3^\mu p_1^\nu)\,,\end{aligned} \tag{3.8}$$

with the form factors A, B and C given by

$$\begin{aligned}A &= \not{p}_1\,B + \not{p}_3\,C\,, \\ B &= (p_2\cdot p_3 + p_3\cdot p_4)\,, \\ C &= (p_1\cdot p_2 + p_1\cdot p_4)\,.\end{aligned} \tag{3.9}$$

One can check that this vertex, satisfies the corresponding Ward identities i.e.,

$$p_{1,\mu}\,\Gamma^{\mu\nu}_{(1,2)} = 0 = p_{3,\nu}\,\Gamma^{\mu\nu}_{(1,2)}\,, \tag{3.10}$$

for both on-shell and off-shell photons. The Feynman rule for the remaining interaction term, involving a Higgs boson, can be trivially obtained from the expression of $\Gamma^{\mu\nu}_{(2)}$.

[3] We would like to point out an erratum in [76] i.e., for the effective photon interaction Lagrangian $\mathcal{L}^Q_{s=1}$. Our expression corresponds to $\mathcal{L}^{\text{eff}}_{(1)}$ from Appendix A, for the particular case $J = 1/2$. On the other hand, we do agree with the expression for the effective four-photon vertex in $\mathcal{L}^Q_{AA}$ which can be obtained from our expression of $\mathcal{L}^{\text{eff}}_{(1)}$ with the substitution $T^{(1/2)} \to T^{(1)}$ and $T^{(1/2)\mu\nu} \to T^{(1)\mu\nu}$ from the same appendix. We can also observe that our result for the $\bar{f}f\gamma\gamma$ vertex (first term from (3.7)) differs in a factor 3 with respect to $\mathcal{L}^Q_{\psi A}$ from the same referred work. Also, as mentioned previously, we shall see that our result does not agree with the expression for the Compton cross section.

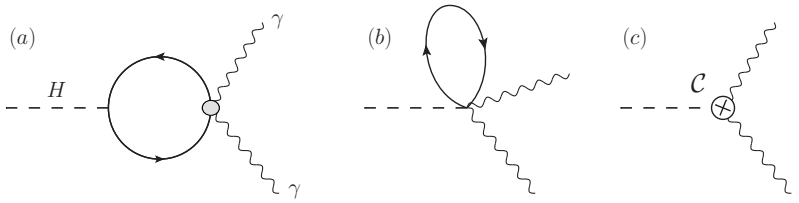

Figure 2. Contributing diagrams to the $H \to \gamma\gamma$ decay from the $\bar{f}f\gamma\gamma$ and $H\bar{f}f\gamma\gamma$ effective interaction vertices and the corresponding renormalization counterterm.

In this analysis we are interested in calculating the $H \to \gamma\gamma$ one loop-induced decay (figure 2) and the $gg \to H$ production cross section. As the previous model is non-renormalizable we have to introduce a counterterm Lagrangian in order to re-absorb the UV divergences generated at the one-loop level for the $H \to \gamma\gamma$ process.[4] We shall parametrize it as

$$\mathcal{L}_Q^{ct} = \mathcal{C}\,\frac{3\beta}{(4\pi)^2 v}\left(\frac{m^4}{\Lambda_Q^4}\right) H F_{\alpha\beta}F^{\alpha\beta}\,, \tag{3.11}$$

as there is a unique (CP-even) dimension 6 effective-operator that satisfies the SM symmetries, that contributes to the corresponding process, and the same is valid for the $gg \to H$ process.

In the following, we shall revise the Compton scattering cross section and afterwards, calculate the new contributions to the $H \to \gamma\gamma$ and $gg \to H$ loop functions, which are, as we shall shortly demonstrate, the only relevant ones, as all the contributions to the remaining channels will turn out to be highly suppressed.

4 Revised Compton Scattering

For Compton scattering at high energies, we can safely work in the massless electron limit. The corrected Compton cross section (with respect to ref. [76]), including the standard QED contributions and the ones corresponding to the additional effective vertex from $\mathcal{L}_Q^{\text{eff}}$ (3.7) is given by

$$\frac{d\sigma_{e\gamma\to e\gamma}}{d\Omega} = \frac{1}{256\pi^2 s}(5+\cos^2\theta+2\cos\theta)\left[\left(\frac{3\beta}{4\Lambda_Q^4}\right)^2 s^4(1+\cos\theta) + \left(\frac{3\beta}{\Lambda_Q^4}\right) s^2 e^2 Q_e^2 + \frac{4\,e^4 Q_e^4}{(1+\cos\theta)}\right], \tag{4.1}$$

where $Q_e = -1$ is the charge of the electron and e is the QED coupling constant. In the phenomenological analysis section (Section 6) we will re-analyse the corresponding experimental Compton scattering data from [85] as in [76] using the previous formula, and obtain bounds on the model parameters.

[4] This proceedure can be trivially expanded to the $gg \to H$ process, but it will not be necessary as one can easily infer the finite expression for this process from the finite loop expression of $H \to \gamma\gamma$.

5 $H \to \gamma\gamma$ Decay Rate and $gg \to H$ Cross Section

As mentioned previously, the three contributions to the $H \to \gamma\gamma$ effective vertex for on-shell photons and Higgs boson are shown in figure 2, where the first diagram contains the $\bar{f}f\gamma\gamma$ effective vertex and the $H\bar{f}f$ Yukawa interaction, the second diagram corresponds to the $H\bar{f}f\gamma\gamma$ term from (3.7) and, the last diagram corresponds to the counter-term. Its expression for one fermion in the loop takes the gauge-invariant form

$$i\,\Gamma^{\mu\nu}_{H\gamma\gamma} = i(\eta^{\mu\nu} M_H^2 - 2q'^{\mu} q^{\nu})\Big(\Pi_F(m, M_H, \mu) + \Pi_\epsilon(m, \mu)\Big)\,, \tag{5.1}$$

where momentum conservation reads $p = q + q'$ and where we have neglected the terms that vanish when contracted with the photon polarization four-vectors $\epsilon_r^\mu(q)$ and $\epsilon_s^\nu(q')$. The Π_ϵ form factor contains an UV-pole, and its expression in the $\overline{\text{MS}}$ scheme is given by

$$\Pi_\epsilon(m^2, \mu^2) = \mu^{2\epsilon} \frac{1}{2\hat{\epsilon}} \left(\frac{m^4}{\Lambda_Q^4}\right) \frac{6\beta}{(4\pi)^2 v}\,, \tag{5.2}$$

where μ is the renormalization scale and $1/\hat{\epsilon} \equiv 1/\epsilon + \gamma_E - \ln(4\pi)$. This terms gets renormalized by the tree-level counter-term Lagrangian (3.11) as follows. We re-express the bare constant $\mathcal{C}$ appearing in the Lagrangian as the sum of the renormalized constant $\mathcal{C}_R(\mu)$ and an UV-divergent part that cancels the one that appears at one-loop in the Π_ϵ form factor i.e.,

$$\mathcal{C} = \mathcal{C}_R(\mu) + \delta^\epsilon_{\mathcal{C}} = \mathcal{C}_R(\mu) - \mu^{2\epsilon} \frac{1}{2\hat{\epsilon}}\,, \tag{5.3}$$

therefore $\mathcal{C}_R(\mu)$ satisfies

$$\mathcal{C}_R(\mu) = \mathcal{C}_R(\mu_0) + \ln(\mu/\mu_0)\,. \tag{5.4}$$

If we assume that this term is identically zero at some scale Λ, such that $\mathcal{C}_R(\Lambda) = 0$ then

$$\mathcal{C}_R(\mu) = \ln(\mu/\Lambda)\,. \tag{5.5}$$

In conclusion, after renormalizing we must make the substitution

$$\Pi_\epsilon(m, \mu) \to \Pi_R(m, \mu) = C_R(\mu) \left(\frac{m^4}{\Lambda_q^4}\right) \frac{6\beta}{(4\pi)^2 v}\,, \tag{5.6}$$

where $C_R(\mu) = \ln(\mu/\Lambda)$.

Going back to the expression (5.1), the finite form factor is given by

$$\begin{aligned}\Pi_F(m, M_H, \mu) = -\frac{3m}{2v} \frac{1}{(4\pi)^2 \Lambda_Q^4} \Bigg(& m(2\alpha + \beta)(6m^2 - M_H^2) - \frac{4}{3}(4\alpha + \beta)\, m^3 \\ & - \beta m \int_0^1 dx \Big[2m^2 + M_H^2(6x(x-1) + 1)\Big] \ln \frac{a^2}{\mu^2} \Bigg)\,,\end{aligned} \tag{5.7}$$

where $a^2 = m^2 + M_H^2 x(x-1)$. After integrating in x, the final expression of the total form-factor renders finite and $\mu-$independent (however, it depends on the scale Λ) i.e.,

$$\begin{aligned}\Pi(m, M_H) &\equiv \Pi_F(m, M_H, \mu) + \Pi_R(m, M_H, \mu) \\ &= \frac{1}{v\,(4\pi)^2}\left(\frac{m^4}{\Lambda_Q^4}\right)\left(\frac{M_H^2}{m^2}(3\alpha+\beta) - (10\alpha+7\beta) + 3\beta\ln\frac{m^2}{\Lambda^2}\right). \end{aligned} \tag{5.8}$$

In our analysis there are two possible natural choices for Λ, that is, either v or Λ_Q. Here, we shall vary the value of Λ_Q in the interval $\Lambda_Q \in [v, 1000]$ GeV (where $v = 246$ GeV) and present the results for the previous two choices, that is, $\Lambda = v$ and $\Lambda = \Lambda_Q$.

Including the SM fermionic and W boson contributions, and extending the previous result to all SM fermions and their corresponding colours, the expression for the total decay width at tree level reads

$$\Gamma(H\to\gamma\gamma) = \frac{G_F\alpha^2 M_H^3}{128\,\pi^3}\left|\sum_f N_c^f Q_f^2 \mathcal{F}(x_f) + \mathcal{G}(x_W) + \frac{4\pi v}{\alpha}\sum_f N_c^f \Pi(m_f, M_H)\right|^2, \tag{5.9}$$

where $x_f = 4m_f^2/M_H^2$ (with m_f the fermion mass), Q_f and N_c^f are the electric charge and the number of colors of the fermion f, and finally $x_W = 4M_W^2/M_H^2$. The explicit expressions for the loop functions are, as usual, given by

$$\mathcal{F}(x) = \frac{x}{2}[4 + (x-1)f(x)]\,, \qquad \mathcal{G}(x) = -2 + 3x + \left(\frac{3}{2}x - \frac{3}{4}x^2\right)f(x)\,, \tag{5.10}$$

with

$$f(x) \;=\; \begin{cases} -4\arcsin^2(1/\sqrt{x})\,, & x \geqslant 1 \\ \left[\ln\left(\frac{1+\sqrt{1-x}}{1-\sqrt{1-x}}\right) - i\pi\right]^2, & x < 1 \end{cases}. \tag{5.11}$$

One should note, that the new contribution has a suppression factor $m^4/(4\pi\Lambda_Q^4)$, but also an enhancement factor (N_c/α), with respect to the SM contributions. The overall effect is a suppression factor proportional to

$$\left(\frac{m^4}{\Lambda_Q^4}\right)\frac{N_c}{4\pi\alpha} \;\sim\; 0.45\,, \tag{5.12}$$

for $\Lambda_Q = 500$ GeV and $m = m_t$. This result can be further enhanced with the α and β parameters and obtain comparable contributions to the SM ones.

Before continuing with our analysis further comments are required. In this study we are going to focus on the $H \to \gamma\gamma$ decay channel and also on the remaining decay modes (WW, ZZ, $\bar{b}b$, $\tau\tau$) but only the ones that are produced through the gg fusion channel, which is affected by the same loop form factor as $H \to \gamma\gamma$. As for the neglected channels (production or decay), as they occur at the tree-level, the non-metricity induced interactions would only bring loop-suppressed corrections, which at this stage (given the current experimental uncertainties) can be safely neglected. For completeness, for a rough estimation of the order of magnitude of these corrections with an illustrative example, see Appendix B.

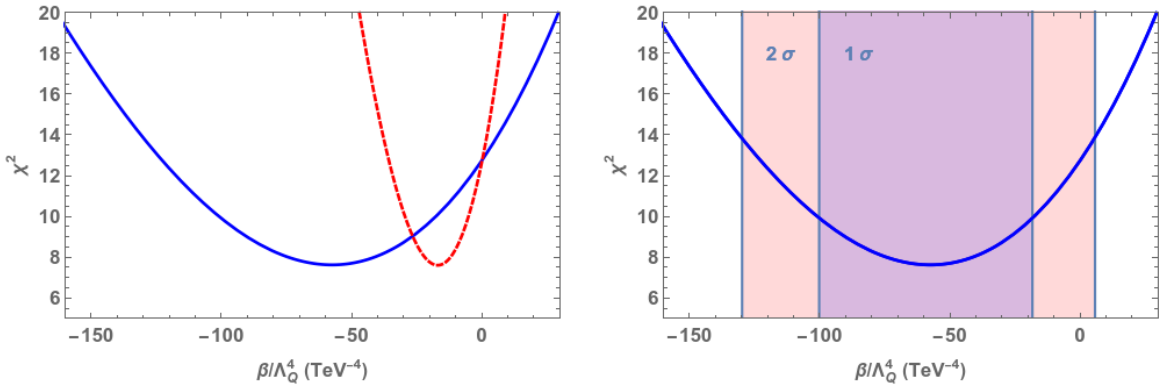

Figure 3. Left: χ^2 function with the correct Compton scattering formula (blue continuous curve) and the previous results from [76] (red-dashed curve). Right: χ^2 function with the correct Compton scattering formula and the corresponding 1σ and 2σ bandwidths.

The same form factors Π_F and Π_R also enter the gluon-fusion process. It can be trivially deduced that the $gg \to H$ cross section, including the non-metricity contributions, will be given by

$$\sigma(gg \to H) = \frac{M_H^2\,\alpha_s^2}{1024\,\pi\,v^2}\left|\sum_q \mathcal{F}(x_q) + \frac{4\pi v}{\alpha_s}\sum_q \Pi(m_q, M_H)\right|^2 \delta(s - M_H^2)\,. \tag{5.13}$$

Both the expression of the gg-fusion production cross section and the one for the $H \to \gamma\gamma$ will be needed in Section 6.2 when defining the LHC signal strengths.

6 Phenomenology

This section will be dedicated to the phenomenological analysis of Compton scattering and the LHC Higgs signal strengths. From both we will obtain useful results with respect to the allowed regions on the parameter space of the model, namely on α, β and Λ_Q. As we shall see in the following, the bounds obtained from the LHC signal strengths are complementary to the ones obtained from Compton scattering, for a generic model where α, β and Λ_Q are free parameters, however, the LHC constraints on the EiBI model will turn out to be the most stringent ones obtained up to date.

6.1 Compton scattering

As previously mentioned, we define a χ^2 estimator including the Compton scattering experimental data [85], as in [76], for the Compton cross section (4.1). The results are shown in Fig. 3. We can observe that the χ^2 curve (blue) grows slower with β/Λ_Q^4 when moving away from the minimum when compared to the previous study [76] (with the incorrect expression for the cross section, red-dashed curve). In the right panel, the 1σ and 2σ regions are also plotted using the correct Compton scattering formula. Depending on the sign of

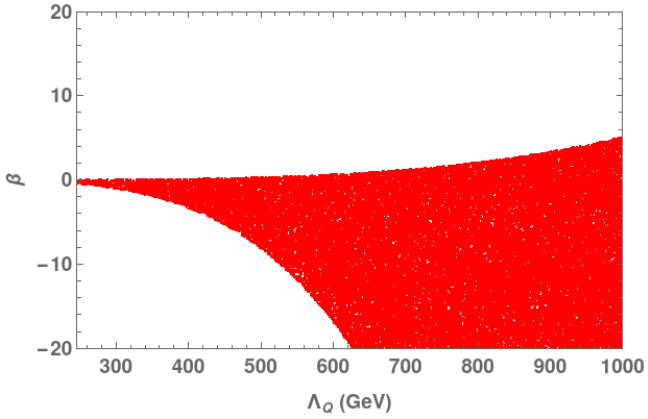

Figure 4. Allowed 2σ region for the (Λ_Q, β) parameter space obtained from the Compton scattering experimental data.

β, at the 2σ level we find

$$\begin{aligned} |\beta|^{-4}\,\Lambda_Q &> 0.29\,\text{TeV} \qquad \text{with } \beta < 0\,, \\ |\beta|^{-4}\,\Lambda_Q &> 0.66\,\text{TeV} \qquad \text{with } \beta > 0\,, \end{aligned} \tag{6.1}$$

which provides a less stringent bound for $\beta < 0$ and a more stringent bound for $\beta > 0$ than previously thought.[5] If, instead, we work in a two-parameter space (Λ_Q, β), we obtain at 2σ level the allowed region shown in figure 4.

6.2 Fits to the LHC data

In order to be able to compare the model predictions with the experimentally measured signal strengths, we define the following ratios for the $H \to \gamma\gamma$ decay channel

$$\mu^X_{\gamma\gamma} \equiv \frac{\sigma^X(pp \to H)\,\text{Br}(H \to \gamma\gamma)}{\sigma^X(pp \to H)_{\text{SM}}\,\text{Br}(H \to \gamma\gamma)_{\text{SM}}}\,, \tag{6.2}$$

where $\sigma^X(pp \to H)$ stands for any specific production cross section. We also define the following ratios

$$\mu^{gg}_Y \equiv \frac{\sigma(gg \to H)\,\text{Br}(H \to Y)}{\sigma(gg \to H)_{\text{SM}}\,\text{Br}(H \to Y)_{\text{SM}}}\,, \tag{6.3}$$

for the $H \to Y$ decays (where Y stands for any measured final state), and where the production channel is gluon fusion.

In conclusion, given the considerations from the previous section, for this fit to the experimental LHC data, we will consider all production channels for the $H \to \gamma\gamma$ decay, and all decay channels for the $\sigma(gg \to H)$ production, as these are the only relevant signal strengths that can suffer sizeable modifications from the new parameters.

[5] The previous results [76] correspond to $|\beta|^{-4}\,\Lambda_Q > 0.39$ TeV for $\beta < 0$ and, $|\beta|^{-4}\,\Lambda_Q > 0.61$ TeV for $\beta > 0$.

Introducing the quotients

$$C_{\gamma\gamma} = \frac{\Gamma(H\to\gamma\gamma)}{\Gamma(H\to\gamma\gamma)_{\rm SM}} = \frac{\left|\sum_f N_c^f Q_f^2 \mathcal{F}(x_f) + \mathcal{G}(x_W) + \dfrac{4\pi v}{\alpha}\sum_f N_c^f \Pi(m_f, M_H)\right|^2}{\left|\sum_f N_c^f Q_f^2 \mathcal{F}(x_f) + \mathcal{G}(x_W)\right|^2},$$

$$C_{gg} = \frac{\sigma(gg\to H)}{\sigma(gg\to H)_{\rm SM}} = \frac{\left|\sum_q \mathcal{F}(x_q) + \dfrac{4\pi v}{\alpha_s}\sum_q \Pi(m_q, M_H)\right|^2}{\left|\sum_q \mathcal{F}(x_q)\right|^2}, \tag{6.4}$$

and the ρ_H function, that allows us to express the total decay of H, including the new interactions, in terms of the SM Higgs width as

$$\Gamma_H = \rho_H\, \Gamma_H^{\rm SM}\,, \tag{6.5}$$

the different signal strengths can be simply expressed as

$$\mu_{\gamma\gamma}^X = C_{\gamma\gamma}\,\rho_H^{-1}\,, \qquad \mu_Y^{gg} = C_{gg}\,\rho_H^{-1}\,, \qquad \text{and} \qquad \mu_{\gamma\gamma}^{gg} = C_{gg}\,C_{\gamma\gamma}\,\rho_H^{-1}\,, \tag{6.6}$$

with $X = VBF,\, VH,\, \bar{t}tH$ and $Y = b\bar{b},\, \tau^+\tau^-,\, VV^*$. For the following fit to the experimental data we shall use a χ^2 estimator using the latest ATLAS and CMS experimental data [3–8, 10–15, 29].

If we choose the scale Λ (at which the effective operator (5.4) is zero, as explained in section 5) as Λ_Q, i.e., $\Lambda = \Lambda_Q$, varying the parameters in the regions

$$\Lambda_Q \in [246,\, 1000]\,\text{GeV}\,, \qquad \alpha \in [-20,\, 20]\,, \qquad \beta \in [-20,\, 20]\,, \tag{6.7}$$

we obtain the 2σ allowed regions shown in figure 5. We observe that there is no correlation between α and Λ_Q (top-left), however, we obtain an upper bound on β, roughly $|\beta| \lesssim 12$ depending on the value of Λ_Q (top-right). On the other hand, we observe a very strong correlation between α and β (bottom-left). This can be easily explained as follows. As the experimental data does not deviate significantly from the SM predictions, the new terms cannot bring large contributions therefore, the two terms must necessarily have opposite signs. Finally, we show the 3D allowed parameter space (bottom-right) which is, roughly, a 2D *surface*.

Similar results can be obtained for $\Lambda = v$ for the same intervals given in (6.7), except we obtain no upper bound for $|\beta|$. The main difference between the two choices of Λ is given by the contribution of the term $\ln(m/\Lambda)$ in (5.8) (with $m = m_t$, the dominant contribution). As this term only gets multiplied by β (and not by a combination of $A\,\alpha + B\,\beta$, as all the other terms that contribute to the form factor) it translates into an effective upper bound on $|\beta|$. We can therefore conclude that, for values of $|\beta| > 12$ the non-metricity contribution to the $\Pi(m, M_H)$ form factor (5.8) becomes more sensitive to (the choice of) the scale Λ.

Once additional bounds are added, such as the previously analysed ones corresponding to Compton scattering, the parameter space, in both cases, gets drastically reduced. We shall specifically analyse these cases in the following section.

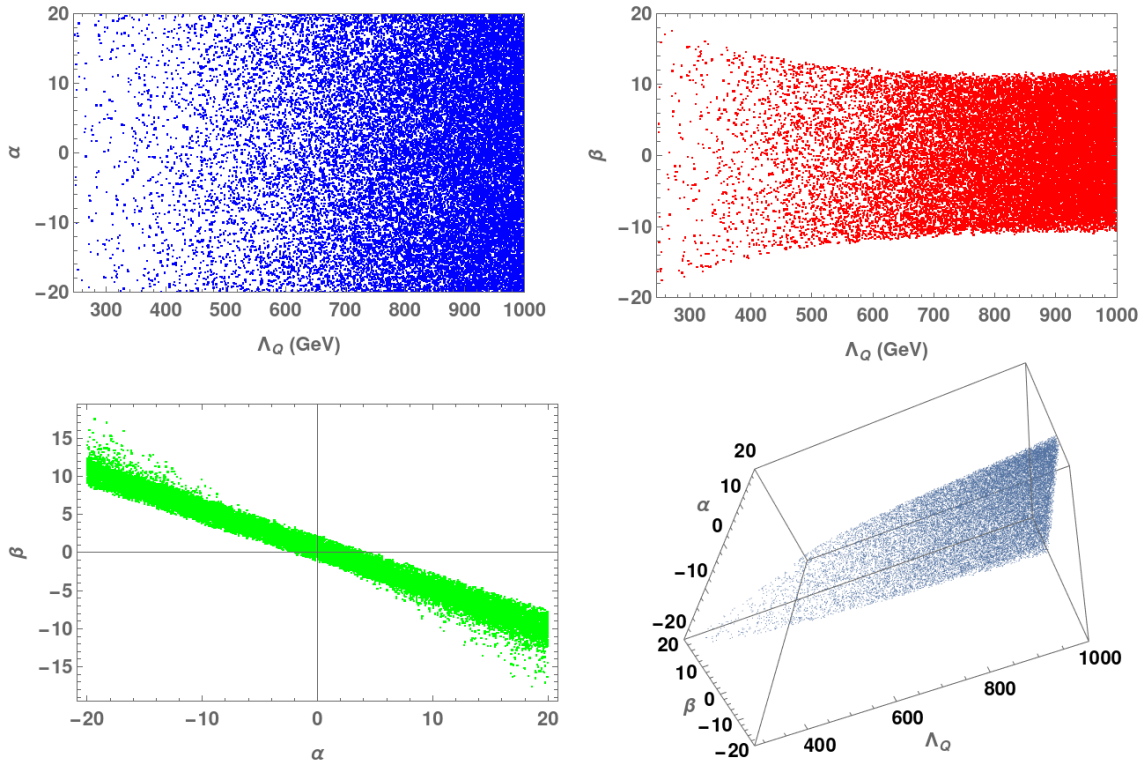

Figure 5. Allowed 2σ regions for different pair combinations of the model parameters (top-left/right and bottom-left), and for all three (bottom-right) for $\Lambda = \Lambda_Q$.

Before moving on, let us shortly turn our attention to the EiBI model and see what are the constraints on this model from the LHC data only. Setting $\alpha = 0$ and $\beta = \pm 1$ we obtain from the χ^2 fit,

$$\begin{aligned} &\Lambda_Q > 835\,\text{GeV} \qquad \text{with} \qquad \Lambda = \Lambda_Q\,, \\ &\Lambda_Q > 980\,\text{GeV} \qquad \text{with} \qquad \Lambda = v\,, \end{aligned} \tag{6.8}$$

for $\beta = -1$ and

$$\begin{aligned} &\Lambda_Q > 800\,\text{GeV} \qquad \text{with} \qquad \Lambda = \Lambda_Q\,, \\ &\Lambda_Q > 690\,\text{GeV} \qquad \text{with} \qquad \Lambda = v\,, \end{aligned} \tag{6.9}$$

for $\beta = 1$. We can, therefore, conclude that the LHC constraints are yet, the most stringent ones obtained on the EiBI model.

6.3 Combined Constraints

In the following, we shall combine the experimental constraints corresponding to the Compton scattering and the LHC data. The 2σ allowed regions are shown in figure 6 for $\Lambda = \Lambda_Q$ and in figure 7 for $\Lambda = v$. As expected, the Compton experimental data places stringent constraints on the (Λ_Q, β) space, and the strong LHC constraint ($\alpha \simeq -\beta$) roughly translates into the fact that the allowed region in the (Λ_Q, β) plane is a *mirror* image of the

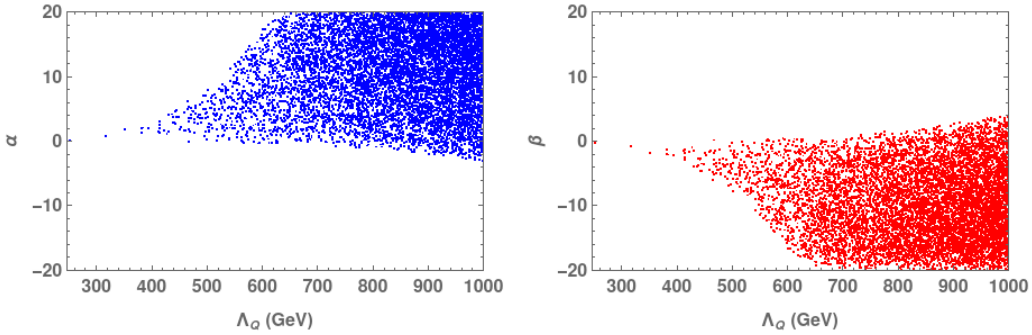

Figure 6. Allowed 2σ regions for $(\alpha,\, \Lambda_Q)$ and $(\beta,\, \Lambda_Q)$ parameter space for $\Lambda = v$.

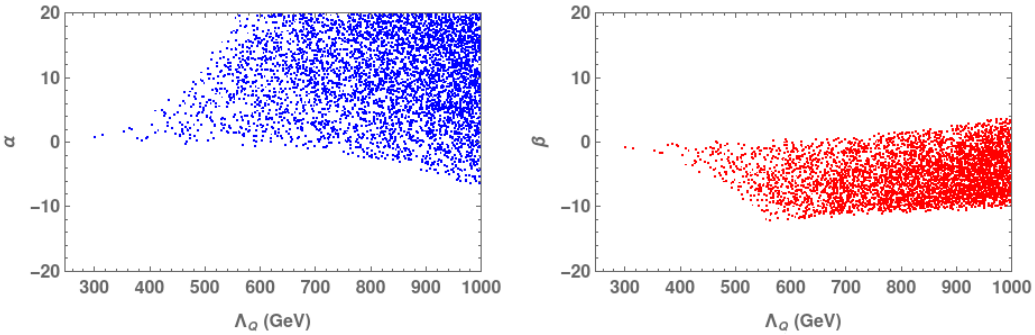

Figure 7. Allowed 2σ regions for $(\alpha,\, \Lambda_Q)$ and $(\beta,\, \Lambda_Q)$ parameter space for $\Lambda = v$.

$(\Lambda_Q,\, \alpha)$ parameter space. For the $\Lambda = \Lambda_Q$ case, however, we can observe that there is a lower bound placed on β, which is given by the LHC data, and it is consistent with the results shown previously in figure 5.

If again, we turn our attention to the EiBI model, as the LHC data sets more stringent bounds on Λ_Q for a one parameter fit, it should be clear that the previously obtained constraints (6.8) and (6.9) also apply for the combined fit.

7 Conclusions

In this manuscript, following the previous works [76, 77] we have studied a model originated by the non-metricity condition of a generic metric, expanding it in inverse powers of the non-metricity scale Λ_Q. As a consequence we have a model with a reduced parameter space with terms that couple to the SM Lagrangian, thus it allows us to experimentally test it at the LHC. At the same time, it allows us to search for evidence of non-Riemannian geometry associated to gravity and gravitational signatures on Higgs-related high energy experiments, which opens a new realm of possible future studies. Finally, we have obtained and discussed relevant bounds on its parameter space (the most stringent up to date).

A Interaction Lagrangian

In this appendix we shall explicitly calculate the corresponding interaction Lagrangians for spin $J = 1/2$, 1, and 0:

$$\begin{aligned}
\mathcal{L}^{\text{eff}}_{(1/2)} &= \frac{i}{4\Lambda_Q^4}\Big[\big[(\mathcal{D}-1)\alpha+\beta\big]\,T^{(1)}\eta^{\mu\nu} - \beta\,T^{(1)\mu\nu}\Big]\Big[\bar\psi\gamma_\mu D_\nu\psi - (D_\nu\bar\psi)\gamma_\mu\psi\Big] \\
&\quad - \frac{m}{2\Lambda_Q^4}\bar\psi\psi(\mathcal{D}\alpha+\beta)T^{(1)}\,, \\
\mathcal{L}^{\text{eff}}_{(1)} &= \frac{1}{8\Lambda_Q^4}F_{\mu\alpha}F_{\nu\beta}\Big[\big[(\mathcal{D}-4)\alpha+\beta\big]\,T^{(1/2)}\eta^{\mu\nu}\eta^{\alpha\beta} - 4\beta\,\eta^{\mu\nu}\,T^{(1/2)\alpha\beta}\Big]\,, \\
\mathcal{L}^{\text{eff}}_{(0)} &= -\frac{m}{v}\frac{(\mathcal{D}\alpha+\beta)}{2\Lambda_Q^4}H\bar\psi\psi\,T^{(1)}\,.
\end{aligned} \tag{A.1}$$

The stress energy tensors for $J = 1/2$ and $J = 1$ can be obtained from (3.1) as usual i.e.,

$$T^{(J)\mu\nu} = -\frac{2}{\sqrt{-g}}\frac{\partial\mathcal{L}^{(J)}}{\partial g^{\mu\nu}}\bigg|_{(\nabla_\mu,\,g_{\mu\nu})\to(D_\mu,\,\eta_{\mu\nu})}\,, \tag{A.2}$$

Its explicit expressions for $J = 1/2$ and $J = 1$ read

$$\begin{aligned}
T^{(1/2)\mu\nu} &= \eta^{\mu\nu}\frac{i}{2}\Big(\bar\psi\overleftrightarrow{\not{D}}\psi\Big) - \eta^{\mu\nu}m\bar\psi\psi \\
&\quad - \frac{i}{2}\Big(\bar\psi(\gamma^\mu D^\nu+\gamma^\nu D^\mu)\psi - (D^\nu\bar\psi)\gamma^\mu\psi - (D^\mu\bar\psi)\gamma^\nu\psi\Big)\,, \\
T^{(1)\mu\nu} &= \eta^{\mu\nu}\frac{1}{4}F_{\alpha\beta}F^{\alpha\beta} - \frac{1}{2}F^{\mu\alpha}F^{\nu}{}_{\alpha} - \frac{1}{2}F^{\nu\alpha}F^{\mu}{}_{\alpha}\,.
\end{aligned} \tag{A.3}$$

The corresponding traces in $\mathcal{D}$ dimensions are given by

$$\begin{aligned}
T^{(1/2)} &= T^{(1/2)\mu}_{\mu} = i\,(\mathcal{D}/2-1)\;\bar\psi\overleftrightarrow{\not{D}}\psi - \mathcal{D}\,m\bar\psi\psi\,, \\
T^{(1)} &= T^{(1)\mu}_{\mu} = (\mathcal{D}/4-1)\,F_{\alpha\beta}F^{\alpha\beta}\,.
\end{aligned} \tag{A.4}$$

Inserting expression (A.3) and (A.4) into (A.1) and summing all three contributions we finally obtain the effective interaction Lagrangian $\mathcal{L}^{\text{eff}}_Q = \mathcal{L}^{\text{eff}}_{(1/2)} + \mathcal{L}^{\text{eff}}_{(1)} + \mathcal{L}^{\text{eff}}_{(0)}$, which reads

$$\begin{aligned}
\mathcal{L}^{\text{eff}}_Q &= \frac{f_1(\mathcal{D},\alpha,\beta)}{\Lambda_Q^4}\frac{i}{2}\Big(\bar\psi\overleftrightarrow{\not{D}}\psi\Big)\,F_{\alpha\beta}F^{\alpha\beta} - \frac{f_2(\mathcal{D},\alpha,\beta)}{\Lambda_Q^4}\,m\bar\psi\psi\,F_{\alpha\beta}F^{\alpha\beta} \\
&\quad + \frac{3\,i\,\beta}{4\Lambda_Q^4}\,F^{\mu\alpha}F^{\nu}{}_{\alpha}\Big(\bar\psi\gamma_\mu D_\nu\psi - (D_\nu\bar\psi)\gamma_\mu\psi\Big) - \frac{m}{v}\frac{f_3(\mathcal{D},\alpha,\beta)}{2\Lambda_Q^4}H\bar\psi\psi\,F_{\alpha\beta}F^{\alpha\beta}\,,
\end{aligned} \tag{A.5}$$

with f_1 and f_2 given by

$$\begin{aligned}
f_1(\mathcal{D},\alpha,\beta) &= \frac{1}{8}\Big[\alpha\,(\mathcal{D}-4)(2\mathcal{D}-3)+\beta\,(2\mathcal{D}-11)\Big] = -\frac{3\beta}{8}+\frac{1}{8}(10\alpha+4\beta)\epsilon+\mathcal{O}(\epsilon^2)\,, \\
f_2(\mathcal{D},\alpha,\beta) &= \frac{1}{4}\,(\mathcal{D}-4)\,(\mathcal{D}\,\alpha+\beta) = \frac{1}{2}(4\alpha+\beta)\epsilon+\mathcal{O}(\epsilon^2)\,, \\
f_3(\mathcal{D},\alpha,\beta) &= (\mathcal{D}\alpha+\beta)\,(\mathcal{D}/4-1) = \frac{1}{2}(4\alpha+\beta)\epsilon+\mathcal{O}(\epsilon^2)\,,
\end{aligned} \tag{A.6}$$

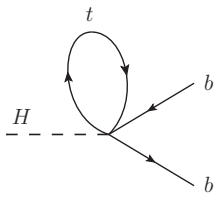

Figure 8. One-loop correction to the $H\bar{b}b$ Yukawa coupling.

where we considered, as mentioned previously $\mathcal{D} = 4+2\epsilon$, expanded in ϵ and kept the $\mathcal{O}(\epsilon)$ terms.

Considering no additional interactions through D_μ i.e., taking $D_\mu \to \partial_\mu$, and using the equations of motion i.e., $(i/2)\bar{\psi}\overleftrightarrow{\partial\!\!\!/}\psi - m\bar{\psi}\psi = 0$ we can further simplify the previous Lagrangian (A.5). We obtain

$$\begin{aligned}\mathcal{L}_Q^{\text{eff}} = \frac{3\,i\,\beta}{4\Lambda_Q^4}\,F^{\mu\alpha}F^{\nu}{}_{\alpha}\left(\bar{\psi}\gamma_\mu\partial_\nu\psi - (\partial_\nu\bar{\psi})\gamma_\mu\psi\right) - \left(\frac{\beta}{2}+\alpha\,\epsilon\right)\frac{3}{4\Lambda_Q^4}m\bar{\psi}\psi\,F_{\alpha\beta}F^{\alpha\beta} \\ - \epsilon\,(4\alpha+\beta)\,\frac{m}{v}\frac{1}{4\Lambda_Q^4}H\bar{\psi}\psi\,F_{\alpha\beta}F^{\alpha\beta}\,,\end{aligned} \tag{A.7}$$

which is the expression that we used in our analysis.

B Loop-induced Yukawa corrections

In order to clarify why the non-metricity contributions are highly suppressed for processes that take place at tree-level let us take the following example. Consider the $\mathcal{L}_{(0)}^{\text{eff}}$ Lagrangian from (A.1), written in a more generic form, as a sum over all SM fermions, and let us also consider that these terms additionally couple to the $T^{(1/2)}$ stress-energy tensor. In this case we obtain an additional interaction Lagrangian $\mathcal{L}_{(0)}^{\prime\text{eff}}$ given by the following expression

$$\begin{aligned}\mathcal{L}_{(0)}^{\prime\text{eff}} &= -\sum_j \frac{m_j}{v}\frac{(\mathcal{D}\alpha+\beta)}{2\Lambda_Q^4}H\bar{\psi}_j\psi_j\,T^{(1/2)} \\ &= -i\sum_j \frac{m_j}{v}\frac{(\mathcal{D}\alpha+\beta)}{2\Lambda_Q^4}H\bar{\psi}_j\psi_j\sum_k\left[\,(\mathcal{D}/2-1)\;\bar{\psi}_k\overleftrightarrow{\not{D}}\psi_k - \mathcal{D}\,m_k\bar{\psi}_k\psi_k\right].\end{aligned} \tag{B.1}$$

If we consider no additional interactions through D_μ and we apply the equations of motion, we obtain

$$\mathcal{L}_{(0)}^{\prime\text{eff}} = \sum_{j,k}\mathcal{C}_{jk}\frac{m_j m_k}{\Lambda_Q^4\,v}H\bar{\psi}_j\psi_j\bar{\psi}_k\psi_k\,. \tag{B.2}$$

If we choose $\psi_j = b$ and $\psi_k = t$ we obtain the dominant loop correction to the $H \to \bar{b}b$ channel as shown in Fig. 8. Thus, the bottom Yukawa coupling receives a correction δ_b as follows

$$\frac{m_b}{v}(1+\delta_b) \qquad \text{with} \qquad \delta_b \sim \frac{1}{(4\pi)^2}\frac{1}{\Lambda_Q^4}\cdot(m_t^4,\; m_t^2M_H^2) \sim \mathcal{O}(10^{-4}) \tag{B.3}$$

for $\Lambda_Q = 500$ GeV, which is extremely small, and, as previously mentioned, can be safely discarded. Similar considerations can be made for the $H \to VV$ channels ($V = W, Z$) and for the different production channels, except of course, for the gluon fusion mechanism which will be taken into consideration.

Acknowledgements

I would like to thank A. Pich for helpful comments on this manuscript.

References

[1] **ATLAS** Collaboration, G. Aad et al., *Observation of a new particle in the search for the Standard Model Higgs boson with the ATLAS detector at the LHC*, *Phys. Lett. B* **716** (2012) 1–29, [arXiv:1207.7214].

[2] **CMS** Collaboration, S. Chatrchyan et al., *Observation of a New Boson at a Mass of 125 GeV with the CMS Experiment at the LHC*, *Phys. Lett. B* **716** (2012) 30–61, [arXiv:1207.7235].

[3] **ATLAS** Collaboration, G. Aad et al., *Measurements of the Higgs boson inclusive and differential fiducial cross-sections in the diphoton decay channel with pp collisions at* $\sqrt{s} = 13$ *TeV with the ATLAS detector*, arXiv:2202.0048.

[4] **ATLAS** Collaboration, G. Aad et al., *Measurements of Higgs boson production cross-sections in the* $H \to \tau^+\tau^-$ *decay channel in pp collisions at* $\sqrt{s} = 13$ *TeV with the ATLAS detector*, arXiv:2201.0826.

[5] **ATLAS** Collaboration, G. Aad et al., *Constraints on Higgs boson production with large transverse momentum using* $H \to b\bar{b}$ *decays in the ATLAS detector*, *Phys. Rev. D* **105** (2022) 092003, [arXiv:2111.0834].

[6] **ATLAS** Collaboration, G. Aad et al., *Constraints on Higgs boson properties using* $WW^*(\to e\nu\mu\nu)jj$ *production in 36.1* fb^{-1} *of* $\sqrt{s}$*=13 TeV pp collisions with the ATLAS detector*, arXiv:2109.1380.

[7] **ATLAS** Collaboration, G. Aad et al., *Measurements of the Higgs boson inclusive and differential fiducial cross sections in the* 4ℓ *decay channel at* $\sqrt{s} = 13$ *TeV*, *Eur. Phys. J. C* **80** (2020), no. 10 942, [arXiv:2004.0396].

[8] **CMS Collaboration** Collaboration, *Measurements of the Higgs boson production cross section and couplings in the WW boson pair decay channel in proton-proton collisions at* $\sqrt{s} = 13$ *TeV*, .

[9] **CMS Collaboration** Collaboration, *Search for Higgs boson decays to a Z boson and a photon in proton-proton collisions at* $\sqrt{s} = 13$ *TeV*, arXiv:2204.1294. Submitted to the Journal of High Energy Physics. All figures and tables can be found at http://cms-results.web.cern.ch/cms-results/public-results/publications/HIG-19-014 (CMS Public Pages).

[10] **CMS Collaboration** Collaboration, *Measurements of Higgs boson production in the decay channel with a pair of* τ *leptons in proton-proton collisions at* $\sqrt{s} = 13$ *TeV*, arXiv:2204.1295. Submitted to the European Physical Journal C. All figures and tables can be found at

http://cms-results.web.cern.ch/cms-results/public-results/publications/HIG-19-010 (CMS Public Pages).

[11] **CMS** Collaboration, *Combined Higgs boson production and decay measurements with up to 137 fb^{-1} of proton-proton collision data at $\sqrt{s}$ = 13 TeV*, .

[12] **CMS** Collaboration, A. M. Sirunyan et al., *Combined measurements of Higgs boson couplings in proton–proton collisions at $\sqrt{s} = 13$ TeV*, *Eur. Phys. J. C* **79** (2019), no. 5 421, [arXiv:1809.1073].

[13] **CMS** Collaboration, A. M. Sirunyan et al., *Observation of Higgs boson decay to bottom quarks*, *Phys. Rev. Lett.* **121** (2018), no. 12 121801, [arXiv:1808.0824].

[14] **CMS** Collaboration, A. M. Sirunyan et al., *Measurement of the inclusive and differential Higgs boson production cross sections in the leptonic WW decay mode at $\sqrt{s}$ = 13 TeV*, *JHEP* **03** (2021) 003, [arXiv:2007.0198].

[15] **CMS** Collaboration, A. M. Sirunyan et al., *Measurements of properties of the Higgs boson decaying into the four-lepton final state in pp collisions at $\sqrt{s} = 13$ TeV*, *JHEP* **11** (2017) 047, [arXiv:1706.0993].

[16] **ATLAS** Collaboration, G. Aad et al., *Measurement of Higgs boson decay into b-quarks in associated production with a top-quark pair in pp collisions at $\sqrt{s} = 13$ TeV with the ATLAS detector*, arXiv:2111.0671.

[17] **CMS Collaboration** Collaboration, A. Tumasyan et al., *First evidence for off-shell production of the Higgs boson and measurement of its width*, arXiv:2202.0692. Submitted to Nature Physics. All figures and tables can be found at http://cms-results.web.cern.ch/cms-results/public-results/publications/HIG-21-013 (CMS Public Pages).

[18] **ATLAS** Collaboration, G. Aad et al., *Measurements of Higgs bosons decaying to bottom quarks from vector boson fusion production with the ATLAS experiment at $\sqrt{s} = 13$ TeV*, *Eur. Phys. J. C* **81** (2021), no. 6 537, [arXiv:2011.0828].

[19] **CMS Collaboration** Collaboration, A. Sirunyan et al., *Constraints on anomalous Higgs boson couplings to vector bosons and fermions in its production and decay using the four-lepton final state*, *Phys. Rev. D* **104** (Apr, 2021) 052004. 51 p, [arXiv:2104.1215]. Replaced with the published version. Added the journal reference and the DOI. All the figures and tables can be found at http://cms-results.web.cern.ch/cms-results/public-results/publications/HIG-19-009 (CMS Public Pages).

[20] **CMS Collaboration** Collaboration, A. M. Sirunyan et al., *Measurements of production cross sections of the Higgs boson in the four-lepton final state in proton-proton collisions at $\sqrt{s}$ = 13 TeV. Measurements of production cross sections of the Higgs boson in the four-lepton final state in proton–proton collisions at $\sqrt{s}$ = 13 TeV*, *Eur. Phys. J. C* **81** (Mar, 2021) 488. 66 p, [arXiv:2103.0495]. Replaced with the published version. Added the journal reference and the DOI. All the figures and tables can be found at http://cms-results.web.cern.ch/cms-results/public-results/publications/HIG-19-001 (CMS Public Pages).

[21] **CMS Collaboration** Collaboration, A. M. Sirunyan et al., *Measurement of the Higgs boson production raATLAS:2018xbv,te in association with top quarks in final states with electrons, muons, and hadronically decaying tau leptons at $\sqrt{s}$ = 13 TeV*, *Eur. Phys. J. C* **81** (Nov,

2020) 378. 51 p, [arXiv:2011.0365]. Replaced with the published version. Added the journal reference and the DOI. All the figures and tables can be found at http://cms-results.web.cern.ch/cms-results/public-results/publications/HIG-19-008 (CMS Public Pages).

[22] **ATLAS** Collaboration, G. Aad et al., *Search for Higgs boson production in association with a high-energy photon via vector-boson fusion with decay into bottom quark pairs at $\sqrt{s}$=13 TeV with the ATLAS detector*, *JHEP* **03** (2021) 268, [arXiv:2010.1365].

[23] **ATLAS** Collaboration, G. Aad et al., *Measurement of the associated production of a Higgs boson decaying into b-quarks with a vector boson at high transverse momentum in pp collisions at $\sqrt{s} = 13$ TeV with the ATLAS detector*, *Phys. Lett. B* **816** (2021) 136204, [arXiv:2008.0250].

[24] **ATLAS** Collaboration, G. Aad et al., *A search for the dimuon decay of the Standard Model Higgs boson with the ATLAS detector*, *Phys. Lett. B* **812** (2021) 135980, [arXiv:2007.0783].

[25] **ATLAS** Collaboration, G. Aad et al., *Combined measurements of Higgs boson production and decay using up to 80 fb^{-1} of proton-proton collision data at $\sqrt{s} = 13$ TeV collected with the ATLAS experiment*, *Phys. Rev. D* **101** (2020), no. 1 012002, [arXiv:1909.0284].

[26] **ATLAS, CMS** Collaboration, L. Cadamuro, *Higgs boson couplings and properties*, *PoS* **LHCP2019** (2019) 101.

[27] **ATLAS** Collaboration, *Measurement of Higgs boson production in association with a $t\bar{t}$ pair in the diphoton decay channel using 139fb^{-1} of LHC data collected at $\sqrt{s} = 13$ ˜TeV by the ATLAS experiment*, .

[28] **ATLAS** Collaboration, M. Aaboud et al., *Observation of Higgs boson production in association with a top quark pair at the LHC with the ATLAS detector*, *Phys. Lett. B* **784** (2018) 173–191, [arXiv:1806.0042].

[29] **CMS** Collaboration, *Measurements of the Higgs boson production cross section and couplings in the W boson pair decay channel in proton-proton collisions at $\sqrt{s}$ = 13 TeV*, arXiv:2206.0946.

[30] R. Contino, M. Ghezzi, C. Grojean, M. Muhlleitner, and M. Spira, *Effective Lagrangian for a light Higgs-like scalar*, *JHEP* **07** (2013) 035, [arXiv:1303.3876].

[31] H. Bahl, E. Fuchs, S. Heinemeyer, J. Katzy, M. Menen, K. Peters, M. Saimpert, and G. Weiglein, *Constraining the CP structure of Higgs-fermion couplings with a global LHC fit, the electron EDM and baryogenesis*, arXiv:2202.1175.

[32] B. Grzadkowski, M. Iskrzynski, M. Misiak, and J. Rosiek, *Dimension-Six Terms in the Standard Model Lagrangian*, *JHEP* **10** (2010) 085, [arXiv:1008.4884].

[33] P. Bechtle, C. Chall, M. King, M. Kraemer, P. Maettig, and M. Stöltzner, *Bottoms Up: Standard Model Effective Field Theory from a Model Perspective*, arXiv:2201.0881.

[34] S. Kanemura and R. Nagai, *A new Higgs effective field theory and the new no-lose theorem*, *JHEP* **03** (2022) 194, [arXiv:2111.1258].

[35] M. Battaglia, M. Grazzini, M. Spira, and M. Wiesemann, *Sensitivity to BSM effects in the Higgs p_T spectrum within SMEFT*, *JHEP* **11** (2021) 173, [arXiv:2109.0298].

[36] I. n. Asiáin, D. Espriu, and F. Mescia, *Introducing tools to test Higgs boson interactions via WW scattering: One-loop calculations and renormalization in the Higgs effective field theory*, *Phys. Rev. D* **105** (2022), no. 1 015009, [arXiv:2109.0267].

[37] V. Bresó-Pla, A. Falkowski, and M. González-Alonso, *A_{FB} in the SMEFT: precision Z physics at the LHC*, *JHEP* **08** (2021) 021, [arXiv:2103.1207].

[38] S. Banerjee, R. S. Gupta, O. Ochoa-Valeriano, M. Spannowsky, and E. Venturini, *A fully differential SMEFT analysis of the golden channel using the method of moments*, *JHEP* **06** (2021) 031, [arXiv:2012.1163].

[39] S. Das Bakshi, J. Chakrabortty, C. Englert, M. Spannowsky, and P. Stylianou, *CP violation at ATLAS in effective field theory*, *Phys. Rev. D* **103** (2021), no. 5 055008, [arXiv:2009.1339].

[40] C. Hays, A. Helset, A. Martin, and M. Trott, *Exact SMEFT formulation and expansion to $\mathcal{O}(v^4/\Lambda^4)$*, *JHEP* **11** (2020) 087, [arXiv:2007.0056].

[41] A. Dobado and D. Espriu, *Strongly coupled theories beyond the Standard Model*, *Prog. Part. Nucl. Phys.* **115** (2020) 103813, [arXiv:1911.0684].

[42] J. J. Sanz-Cillero, A. Pich, and I. Rosell, *Electroweak effective theory and beyond Standard Model resonances*, *Nucl. Part. Phys. Proc.* **312-317** (2021) 196–200, [arXiv:2012.1263].

[43] A. Pich, I. Rosell, and J. J. Sanz-Cillero, *Bottom-up approach within the electroweak effective theory: Constraining heavy resonances*, *Phys. Rev. D* **102** (2020), no. 3 035012, [arXiv:2004.0282].

[44] A. Pich, *Effective Field Theory with Nambu-Goldstone Modes*, arXiv:1804.0566.

[45] A. Pich, *Effective field theory: Course*, in *Les Houches Summer School in Theoretical Physics, Session 68: Probing the Standard Model of Particle Interactions*, pp. 949–1049, 6, 1998. hep-ph/9806303.

[46] **LIGO Scientific, Virgo** Collaboration, B. P. Abbott et al., *Observation of Gravitational Waves from a Binary Black Hole Merger*, *Phys. Rev. Lett.* **116** (2016), no. 6 061102, [arXiv:1602.0383].

[47] **LIGO Scientific, Virgo** Collaboration, B. P. Abbott et al., *Binary Black Hole Mergers in the first Advanced LIGO Observing Run*, *Phys. Rev. X* **6** (2016), no. 4 041015, [arXiv:1606.0485]. [Erratum: Phys.Rev.X 8, 039903 (2018)].

[48] **LIGO Scientific, Virgo** Collaboration, B. P. Abbott et al., *GW151226: Observation of Gravitational Waves from a 22-Solar-Mass Binary Black Hole Coalescence*, *Phys. Rev. Lett.* **116** (2016), no. 24 241103, [arXiv:1606.0485].

[49] **LIGO Scientific, VIRGO** Collaboration, B. P. Abbott et al., *GW170104: Observation of a 50-Solar-Mass Binary Black Hole Coalescence at Redshift 0.2*, *Phys. Rev. Lett.* **118** (2017), no. 22 221101, [arXiv:1706.0181]. [Erratum: Phys.Rev.Lett. 121, 129901 (2018)].

[50] **LIGO Scientific, Virgo** Collaboration, B. P. Abbott et al., *GW170814: A Three-Detector Observation of Gravitational Waves from a Binary Black Hole Coalescence*, *Phys. Rev. Lett.* **119** (2017), no. 14 141101, [arXiv:1709.0966].

[51] **LIGO Scientific, Virgo** Collaboration, B. . P. . Abbott et al., *GW170608: Observation of a 19-solar-mass Binary Black Hole Coalescence*, *Astrophys. J. Lett.* **851** (2017) L35, [arXiv:1711.0557].

[52] **LIGO Scientific, Virgo** Collaboration, B. P. Abbott et al., *GWTC-1: A Gravitational-Wave Transient Catalog of Compact Binary Mergers Observed by LIGO and Virgo during the First and Second Observing Runs*, *Phys. Rev. X* **9** (2019), no. 3 031040, [arXiv:1811.1290].

[53] **LIGO Scientific, VIRGO, KAGRA** Collaboration, R. Abbott et al., *GWTC-3: Compact Binary Coalescences Observed by LIGO and Virgo During the Second Part of the Third Observing Run*, arXiv:2111.0360.

[54] **LIGO Scientific, Virgo** Collaboration, R. Abbott et al., *GWTC-2: Compact Binary Coalescences Observed by LIGO and Virgo During the First Half of the Third Observing Run*, *Phys. Rev. X* **11** (2021) 021053, [arXiv:2010.1452].

[55] Y. Mao, M. Tegmark, A. H. Guth, and S. Cabi, *Constraining Torsion with Gravity Probe B*, *Phys. Rev. D* **76** (2007) 104029, [gr-qc/0608121].

[56] R. T. Hammond, *Torsion gravity*, *Rept. Prog. Phys.* **65** (2002) 599–649.

[57] F. Gronwald and F. W. Hehl, *On the gauge aspects of gravity*, gr-qc/9602013.

[58] V. C. De Andrade, L. C. T. Guillen, and J. G. Pereira, *Teleparallel gravity: An Overview*, gr-qc/0011087.

[59] F. W. Hehl, P. von der Heyde, G. D. Kerlick, and J. M. Nester, *General relativity with spin and torsion: Foundations and prospects*, *Rev. Mod. Phys.* **48** (Jul, 1976) 393–416.

[60] T. Watanabe and M. J. Hayashi, *General relativity with torsion*, gr-qc/0409029.

[61] S. Capozziello, G. Lambiase, and C. Stornaiolo, *Geometric classification of the torsion tensor in space-time*, *Annalen Phys.* **10** (2001) 713–727, [gr-qc/0101038].

[62] M. Gasperini, *Spin-dominated inflation in the einstein-cartan theory*, *Phys. Rev. Lett.* **56** (Jun, 1986) 2873–2876.

[63] I. L. Shapiro, *Physical aspects of the space-time torsion*, *Phys. Rept.* **357** (2002) 113, [hep-th/0103093].

[64] P. Baekler and F. W. Hehl, *Rotating Black Holes in Metric-Affine Gravity*, *Int. J. Mod. Phys. D* **15** (2006) 635–668, [gr-qc/0601063].

[65] J. W. Maluf, *Dirac spinor fields in the teleparallel gravity: Comment on "metric-affine approach to teleparallel gravity"*, *Phys. Rev. D* **67** (May, 2003) 108501.

[66] A. Saa, *Einstein-Cartan theory of gravity revisited*, gr-qc/9309027.

[67] F. W. Hehl, J. D. McCrea, E. W. Mielke, and Y. Ne'eman, *Metric affine gauge theory of gravity: Field equations, Noether identities, world spinors, and breaking of dilation invariance*, *Phys. Rept.* **258** (1995) 1–171, [gr-qc/9402012].

[68] A. Delhom, *Minimal coupling in presence of non-metricity and torsion*, *Eur. Phys. J. C* **80** (2020), no. 8 728, [arXiv:2002.0240].

[69] J. E. G. Silva, R. V. Maluf, G. J. Olmo, and C. A. S. Almeida, *Braneworlds in $f(Q)$ gravity*, arXiv:2203.0572.

[70] V. I. Afonso, C. Bejarano, R. Ferraro, and G. J. Olmo, *Determinantal Born-Infeld coupling of gravity and electromagnetism*, *Phys. Rev. D* **105** (2022), no. 8 084067, [arXiv:2112.0997].

[71] E. N. Saridakis, R. Lazkoz, V. Salzano, P. Vargas Moniz, S. Capozziello, J. Beltrán Jiménez, M. De Laurentis, and G. J. Olmo, eds., *Modified Gravity and Cosmology*. Springer, 2021.

[72] V. I. Afonso, G. J. Olmo, and D. Rubiera-Garcia, *Mapping Ricci-based theories of gravity into general relativity*, *Phys. Rev. D* **97** (2018), no. 2 021503, [arXiv:1801.1040].

[73] J. Beltran Jimenez, L. Heisenberg, G. J. Olmo, and D. Rubiera-Garcia, *Born–Infeld inspired modifications of gravity*, *Phys. Rept.* **727** (2018) 1–129, [arXiv:1704.0335].

[74] P. Pani, T. Delsate, and V. Cardoso, *Eddington-inspired Born-Infeld gravity. Phenomenology of non-linear gravity-matter coupling*, *Phys. Rev. D* **85** (2012) 084020, [arXiv:1201.2814].

[75] G. J. Olmo and D. Rubiera-Garcia, *Some Recent Results on Ricci-Based Gravity Theories*, arXiv:2203.0411.

[76] A. Delhom, V. Miralles, and A. Peñuelas, *Effective interactions in Ricci-Based Gravity below the non-metricity scale*, *Eur. Phys. J. C* **80** (2020), no. 4 340, [arXiv:1907.0561].

[77] A. D. I. Latorre, G. J. Olmo, and M. Ronco, *Observable traces of non-metricity: new constraints on metric-affine gravity*, *Phys. Lett. B* **780** (2018) 294–299, [arXiv:1709.0424].

[78] J. Ellis, N. E. Mavromatos, and T. You, *Light-by-Light Scattering Constraint on Born-Infeld Theory*, *Phys. Rev. Lett.* **118** (2017), no. 26 261802, [arXiv:1703.0845].

[79] J. Beltrán Jiménez, A. Delhom, G. J. Olmo, and E. Orazi, *Born-Infeld gravity: Constraints from light-by-light scattering and an effective field theory perspective*, *Phys. Lett. B* **820** (2021) 136479, [arXiv:2104.0164].

[80] I. Antoniadis and E. T. Tomboulis, *Gauge invariance and unitarity in higher-derivative quantum gravity*, *Phys. Rev. D* **33** (May, 1986) 2756–2779.

[81] D. Johnston, *Sedentary ghost poles in higher derivative gravity*, *Nuclear Physics B* **297** (1988), no. 4 721–732.

[82] R. P. Woodard, *Ostrogradsky's theorem on Hamiltonian instability*, *Scholarpedia* **10** (2015), no. 8 32243, [arXiv:1506.0221].

[83] J. Beltrán Jiménez and A. Delhom, *Ghosts in metric-affine higher order curvature gravity*, *Eur. Phys. J. C* **79** (2019), no. 8 656, [arXiv:1901.0898].

[84] W. H. Erskine, *The Born-Infeld theory of electromagnetism*, *Bull. Am. Math. Soc.* **41** (1935), no. 1 28.37.

[85] **L3** Collaboration, P. Achard et al., *Compton scattering of quasi-real virtual photons at LEP*, *Phys. Lett. B* **616** (2005) 145–158, [hep-ex/0504012].